Proceedings of the Twenty-seventh (2017) International Ocean and Polar Engineering Conference **www.isope.org**
San Francisco, CA, USA, June 25-30, 2017

ISBN 978-1-880653-97-5; ISSN 1098-6189

CFD Study of VIM of a Paired-Column Semi-Submersible Platform

*Weiwen Zhao, Decheng Wan**
Collaborative Innovation Center for Advanced Ship and Deep-Sea Exploration, State Key Laboratory of Ocean Engineering, School of Naval Architecture, Ocean and Civil Engineering, Shanghai Jiao Tong University, Shanghai, China
*Corresponding author

ABSTRACT

The Paired-Column Semi-Submersible platform(PC Semi) is a deep-draft semi-submersible (DDS) designed by Houston Offshore Engineering (HOE). It has 8 columns instead of 4 columns compared with conventional DDS. In this paper, the VIM characteristics of PC Semi was numerically investigated by our in-house CFD solver naoe-FOAM-SJTU. Drag test and free-decay tests was carried out first, then VIM tests at different reduced velocities were performed. Shear-stress transport based delayed detached-eddy simulation (SST-DDES) was used for modeling the massively separated turbulent flows. To illustrate the benefit of SST-DDES model, an extra unsteady Reynolds-Average Navier-Stokes (URANS) simulation was computed for drag test. Drag, flow fields and vortical structures were compared with those obtained by SST-DDES. For VIM tests, the dynamic overset grid technique was applied to handle the motions of platform. Results showed that the current CFD approach is applicable and reliable for VIM and can be an alternative for model testing.

KEY WORDS: Deep-draft semi-submersible; reduced velocity; lock-in; vortex-induced motions; naoe-FOAM-SJTU solver

INTRODUCTION

The origins of semi-submersible floating production systems can date back to 1960s. Till today semis are widely installed in offshore oil and gas fields all over the world. In deep water oil drilling production environment, semis are often favored for their low dynamic response to waves in surge and sway. While for conventional semi, large wave-induced heave motion is always a great challenge to the strength and fatigue of its riser and mooring system. To overcome this issue and reduce heave motion, one common improvement is to increase the draft of platform. Deep draft semi-submersible (DDS) is of course such an attractive solution and preferred by offshore industry. The deep draft hull forms can mitigate large heave motion. However, it introduces a new issue, the vortex-induced motions (VIM). VIM is actually the result of transverse fluctuating pressure caused by periodic vortex shedding on long vertical hull of platforms. The periodic sway motions will also accelerate the fatigue failure for riser and mooring system.

Researches for Spar VIM have been put forward since 2003 (Dijk et al., 2003a, 2003b), while it began more recently for VIM of semis. Experimental research on VIM of conventional semis were presented by, for instance, Waals et al. (2007), Gonçalves et al. (2011), Magee et al. (2011), and more recently for DDS by Zou et al. (2013), Antony et al. (2015a). In these model tests, the scale ratios of various hull forms were in the order of 1:70 to 1:50, with small scale exceptions (Gonçalves et al., 2011; Zou et al., 2013). Thanks to the advancement of computational science and turbulence modeling, Computational Fluid Dynamics (CFD) is becoming feasible and practical to evaluate VIM characteristics in the design phase (Kim et al., 2011; Antony et al., 2015b; Chen and Chen, 2016; Kara et al., 2016). Unlike Spar VIM, which considers only surge and sway as its dominant degrees-of-freedom (DOF) motions, DDS VIM takes an extra rotation motion, namely the yaw motion. The extra rotation motion of DDS VIM makes the wake interference between columns more complex, which conversely affect the dynamic VIM response.

The non-dimensioned reduced velocity, along with the Strouhal number, are the most important parameters to characterize VIM motions. These two parameters are defined as

$$U_r \equiv \frac{U}{f_n D} \tag{1}$$

$$St \equiv \frac{f_s D}{U} \tag{2}$$

Where, U is flow velocity, f_n is the natural (transverse) frequency of the system, f_s is the vortex shedding frequency, D is characteristic length. Experiments by Norberg (1987; 1994) showed the Strouhal number for circular cylinder is 0.21. Norberg (1993) also experimentally investigated flow past fixed rectangular cylinder at different incident angles from 0° to 90° and found out that the Strouhal numbers for 0°and 45° incident angles were 0.13 and 0.17, respectively, in a wide range of Reynolds numbers. For a fixed cylinder with constant incident angle, the shedding frequency is proportional to flow velocity. If the cylinder is elastically mounted and allowed to oscillate, when shedding frequency is approaching to one natural sway frequency,

strong modulated oscillating sway motion will occur as a result of resonance. The phenomenon is called "lock-in" and will have great impact on fatigue failure of riser and mooring system. When "lock-in" happens, U_r is around the reciprocal of St, which is typically in range 5~8 for various Strouhal numbers.

The paired-column semi-submersible (PC Semi) is a conceptual design for dry-tree application by Houston Offshore Engineering (HOE). The objective of this design is to provide an alternative of Spar platform in the Gulf of Mexico (GoM). It can provide large payload capability than Spar, while maintain the low dynamic response comparing with conventional semi. Distinguished from conventional DDS, the PC Semi has 8 columns rather than 4, with rectangular column section shape rather than square (Zou et al., 2013). Moreover, it has a higher aspect ratio (immersed length H to diameter or width D of column) which could induce significant VIM. The 8 columns are divided into inner columns and outer columns. The outer columns have larger section area and are connected to inner columns at four corners. This unprecedented design should result in unique VIM response and be carefully investigated. Prior works to investigate VIM characteristics of the PC Semi have been presented as parts of the Research Partnership to Secure Energy for America (RPSEA) 4405 and 5404 projects. Meanwhile, a large number of experimental and numerical data have been published (Zou et al., 2013; Antony et al., 2015b, 2015a; Kim et al., 2015; Vinayan et al., 2015; Kara et al., 2016).

In the present paper, the VIM characteristics of PC Semi in "lock-in" range was numerically investigated by our CFD solver naoe-FOAM-SJTU. The paper is organized as follows: the numerical methods of the present work is introduced first; followed by the description of PC Semi geometry and case conditions of all running tests; then the results, including drag tests, free-decay tests and VIM tests are given; finally some conclusions are drawn.

NUMERICAL APPROACHES

The naoe-FOAM-SJTU Solver

The naoe-FOAM-SJTU solver is a finite volume CFD solver developed based on the open source framework OpenFOAM, with specifically integrated functionality targeting simulation of ship and ocean engineering hydrodynamics (Shen et al., 2012; Shen and Wan, 2013). It consists of a six-degree-of-freedom (6DOF) motion module, a wave generation and absorption module and a mooring system module. The solver was extended to have fully parallelized dynamic overset grid capability (Shen et al., 2015) to address complex dynamic motions problems for ships and offshore floating structures, and detached-eddy simulation (DES) turbulence modelling strategy (Zhao and Wan, 2016a, 2016b) to address massively separated turbulent flows.

Turbulence Modelling

In the present study, the shear stress transport (SST) based delayed DES (DDES) method is applied to address the accuracy for massively separated unsteady flow at high Reynolds numbers. The SST-DDES is a hybrid RANS-LES method that functions like SST k-ω RANS model in the near wall attached boundary region, and like LES subgrid-scale model in the separated free shear flow region. For incompressible viscous fluid, the averaged or filtered continuity equation, as well as Navier-Stokes equation is given by

$$\frac{\partial \overline{u}_i}{\partial x_i} = 0 \tag{3}$$

$$\frac{\partial \overline{u}_i}{\partial t} + \frac{\partial \overline{u}_j \overline{u}_i}{\partial x_j} = -\frac{\partial \overline{P}}{\partial x_i} + \frac{\partial}{\partial x_j}\left[\nu\left(\frac{\partial \overline{u}_i}{\partial x_j} + \frac{\partial \overline{u}_j}{\partial x_i}\right)\right] - \frac{\partial \tau_{ij}}{\partial x_j} \tag{4}$$

Where, ν is the molecular viscosity, τ_{ij} is the Reynolds stress tensor or subgrid-scale stress tensor. According Boussinesq hypothesis, τ_{ij} can be expressed as

$$\tau_{ij} = \frac{2}{3}\delta_{ij}k - \nu_t\left(\frac{\partial \overline{u}_i}{\partial x_j} + \frac{\partial \overline{u}_j}{\partial x_i}\right) \tag{5}$$

SST-DDES assumes the eddy viscosity ν_t is a function of turbulent kinetic energy k and specific turbulence dissipation rate ω, and strain invariant S (Menter et al., 2003)

$$\nu_t = \frac{a_1 k}{\max(a_1\omega, SF_2)} \tag{6}$$

In which, k and ω are obtained by the following transport equations

$$\frac{\partial k}{\partial t} + \frac{\partial (u_j k)}{\partial x_j} = \tilde{G} - \frac{k^{3/2}}{l_{DDES}} + \frac{\partial}{\partial x_j}\left[(\nu + \alpha_k \nu_t)\frac{\partial k}{\partial x_j}\right] \tag{7}$$

$$\frac{\partial \omega}{\partial t} + \frac{\partial (u_j \omega)}{\partial x_j} = \gamma S^2 - \beta\omega^2 + \frac{\partial}{\partial x_j}\left[(\nu + \alpha_\omega \nu_t)\frac{\partial \omega}{\partial x_j}\right] + (1 - F_1)CD_{k\omega} \tag{8}$$

The l_{DDES} in k-equation is mixing length scale which control the switch of solution between RANS and LES (Zhao and Wan, 2016a).

Dynamic Overset Grid

The overset grid assembly Suggar++ (Noack et al., 2009) is utilized to compute the domain connectivity information (DCI) which contains the marked hole, fringe, donor cells and interpolating weighting factors. Fully parallelized scheme is achieved by running OpenFOAM and Suggar++ simultaneously at different processors. Grid motion and DCI are communicated between OpenFOAM and Suggar++ processors with message passing interface (MPI). Detailed implementation of the coupling between OpenFOAM and Suggar++ can refer to Shen et al. (2015).

Mooring System

Mooring system is an important aspect for VIM simulations. In model tests, the common way to restrain model is using air bearing system with horizontal mooring system. The air bearing system ensures that the model can move freely in the horizontal plane. In numerical simulation, the mooring system is usually represented by four soft spring lines uniformly distributed around the model to provide isotropic restore stiffness. By such configuration, the model is restrained in the horizontal plane and is allowed to move in only three DOFs, namely surge, sway and yaw. The whole system can be regarded as spring-mass-damper system, whose natural sway frequency is given by

$$f_n = \frac{1}{2\pi}\sqrt{\frac{K}{m+M}} \tag{9}$$

In a similar way, the natural yaw frequency is given by

$$f_{nt} = \frac{1}{2\pi}\sqrt{\frac{K_t}{J + J_a}} \tag{10}$$

Here, K and K_t are effective linear and torsional (rotational) stiffness provided by the mooring system. m and J are mass and moment of inertia, respectively. M and J_a represent the added mass and added moment of inertia of the model in water.

To model the mooring system, a common simplified approach is to treat the system in three uncoupled DOFs. The motion equations in surge, sway and yaw are given by

$$M\ddot{x}(t) + C_x\dot{x}(t) + K_x x(t) = F_x(t) \tag{11}$$

$$M\ddot{y}(t) + C_y\dot{y}(t) + K_y y(t) = F_y(t) \tag{12}$$

$$J\ddot{\theta}(t) + C_t\dot{\theta}(t) + K_t\theta(t) = M_z(t) \tag{13}$$

Where, C_x , C_y and C_t are structural damping coefficients, $x(t)$, $y(t)$ and $\theta(t)$ are surge, sway and yaw, respectively. $F_x(t)$, $F_y(t)$ and $M_z(t)$ are total hydrodynamic forces in X, Y directions and moment in Z direction. The global stiffness in three directions, K_x , K_y and K_t are directly given individually and do not interfere with each other.

This study provides a more general way to model the mooring system, by considering the coupling effects of stiffness amongst surge, sway and yaw directions. Fig. 1 illustrates the plane view of the mooring system in numerical simulation. Four pretensioned springs are horizontally connected between fairleads and anchors. To achieve isotropic stiffness, the four springs are set with same length, stiffness and pretension, and are uniformly distributed around platform. Moreover, fairleads are attached to a virtual ring that moves and rotates with platform. Anchors are fixed in the inertial coordinate system.

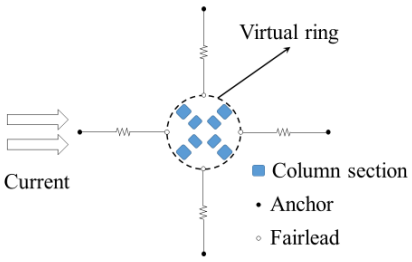

Fig. 1. Schematic of the mooring system

It should be noted that all springs must be pretensioned all over the VIM simulation. The procedure for computing mooring force can be summarized as follows:

(1) Compute the rest length for each spring according to initial position of anchor and fairlead, spring stiffness and pretension;
(2) Compute the position of fairlead in current step according to the motion state of platform;
(3) Compute the elongation, then mooring force by Hooke's law for each spring.

The total mooring forces and moments are then obtained and added to the platform's 6DOF motion equations (Shen and Wan, 2013) as external forces and moments. Although 6DOF motion equations are solved in the simulation, the platform's DOFs is constrained in surge, sway and yaw motions.

As the effective stiffness is provided by four linear springs instead of directly given, it is critical to make sure the effective stiffness in numerical simulation is identical with that in model test. To verify the effective stiffness, static offset tests and free-decay tests should be performed. In static offset tests, the platform is prescribed to move in Y axis and Z rotation directions, respectively, without solving flow field. Parameters such as stiffness and pretension of each spring are then carefully adjusted to match the global stiffness with one provided by model test. A small Python utility was written to achieve this functionality. The free-decay tests allow platform oscillating at an initial offset or velocity in the absence of inflow. Two tests, namely sway and yaw decay test were conducted separately to verify the natural sway and yaw period of the mooring system is equal to the model test.

GEOMETRY AND CONDITIONS

PC Semi Geometry

The PC Semi is an eight column design with four outer columns and four inner columns. Table 1 lists the summary of geometry for full scale PC Semi. The overall height and width of the platform are 82.6m and 113.4m, respectively. The column and pontoon height are 74.4m and 8.2m. The designed draft is 53.3m, which means the submerged column height H is 45.1m. The columns are rounded at four corners with radius of 2.4m. Scale ratio of the model in experiment is 1:54. We select the effective diameter of outer column D=19.4m (0.36m for model scale) as the characteristic width L, resulting an aspect ratio H/L of 2.32. The reduced velocity is also computed based on D, which is consistent with Antony et al. (2015b).

Table 1. Geometry parameters for PC Semi prototype

Parameter	Imperial	SI
Draft	175 ft	53.3 m
Width	372 ft	113.4 m
Outer column space	315 ft	96.0m
Inner column space	165 ft	50.3 m
Outer column width	46 ft x 44 ft	14.0 m x 13.40 m
Inner column width	46 ft x 34 ft	14.0 m x 10.4 m
Column height	244 ft	74.4 m
Pontoon width	42 ft	12.8 m
Pontoon height	27 ft	8.2 m

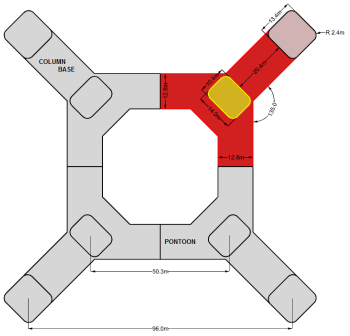

Fig. 2. Plane view of PC Semi (Vinayan et al., 2015)

Table 2. Mass and stiffness related parameters (Kara et al., 2016)

Parameter	Prototype	Model
Scale ratio	1:1	1:54
Mass	79097 t	490.2 kg
Radius of Gyration	41.88 m	0.77593 m
Surge/Sway stiffness	520 kN/m	0.17398 kN/m
Yaw stiffness	55260 kN·m/deg	0.00523 kN·m/deg
Natural sway period	113.5 s	15.45 s
Natural yaw period	68.5 s	9.32 s

Computational Mesh

We utilized unstructured multi-block overset grids in our simulation. Fig. 3 shows the computational domain and overset grid distribution. The grid consists of two overlapping grid blocks, the hull grid and background grid. The hull grid can translate and rotate along with platform's surge, sway and yaw motions in horizontal plane, while the background grid remains fixed during simulation. The computational domain extends to $-14D \le x \le 28D$, $-11D \le y \le 11D$ and $-10D \le z \le 0$. All grid blocks were generated by *snappyHexMesh*. Background grid has a uniform grid spacing of 0.45*D*. The fringe cell size in hull grid is consistent with background grid size such that orphans (cells do not have donor cell from other grid blocks) will not occur during hole-cutting. Grids in wake regions have been octree-based refined at level 3, resulting in a grid size of 0.05625*D*. Boundary layer has four prism cell layers, with the first layer thickness of 0.0024m to make sure *y*+ for first layer is less than 5. The final grid numbers for background and hull block are 0.09M and 2.43M, respectively.

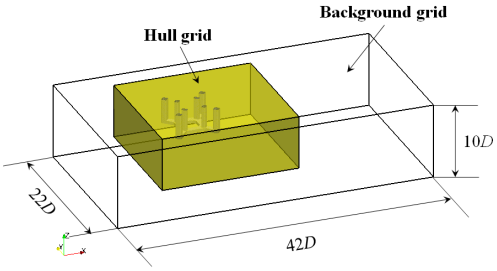

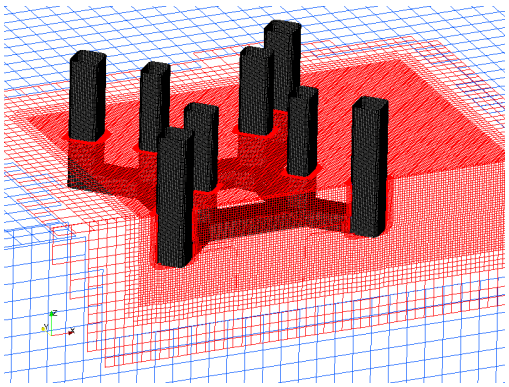

Fig. 3. Computational domain and overset grid

For background mesh, Neumann boundary condition for velocity (fixed inlet) and Dirichlet boundary condition for pressure (zero gradient) were used on the upstream inlet patch ($x = -14D$), and vice versa for downstream outlet patch. Symmetry was applied for top boundary and slip for the remaining boundaries. Typical simulation covers 300s simulation time or 20 oscillation period, which corresponding to 15000 time steps with a time step of 0.02s. Wall clock time for each time step varies from 11s to 15s when running on a Linux cluster using two nodes or 40 CPUs.

RESULTS AND DISCUSSION

Drag Test

The effect of different turbulence modeling strategies are discussed in drag test. Besides SST-DDES, we select SST-URANS to perform drag test for comparison. The platform is stationary and do not allowed to move. The current velocity is 0.272 m/s (corresponding to 2.0 m/s for full scale). Table 3 shows the drag coefficient ($F_x/(\rho U^2)$) of experiment and simulations. SST-URANS overpredicts drag in comparison with SST-DDES, which is in accordance with Zhao and Wan (2016c).

Table 3. Drag parameter of SST-DDES and SST-URANS

Experiment	SST-DDES	SST-URANS
0.91 (±3.0%)	0.913	0.971

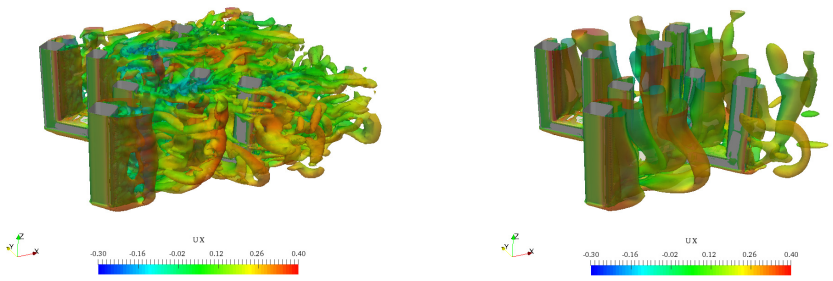

(a) SST-DDES (b) SST-URANS

Fig. 4. Instantaneous vorticity represented by Q-criterion

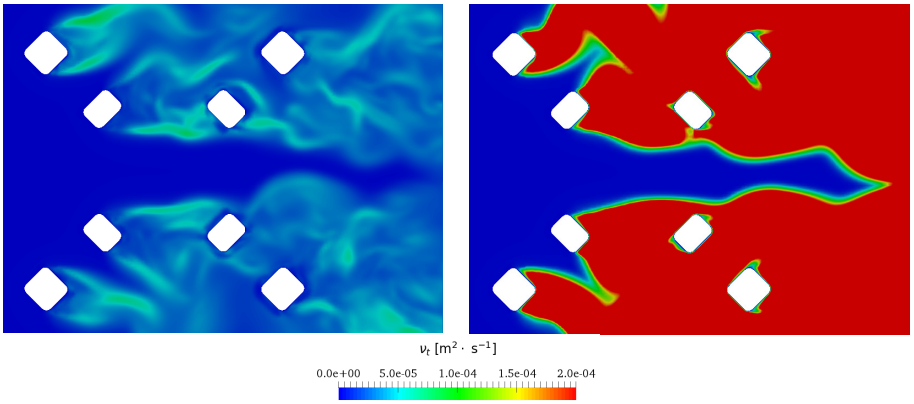

(a) SST-DDES (b) SST-URANS

Fig. 5. Eddy viscosity contour on z=-0.5m slice

Fig. 4 is the flow visualization of vorticity represented by Q-criterion. The figure reveals that SST-DDES captured the coherent vortex structures in the wake region well, which is not shown in URANS computation.

Fig. 5 shows the contour of eddy viscosity on the plane at z=-0.5m. It varies from 0 in blue to $2\times10^{-4}m^2/s$ in red. SST-URANS overestimates turbulent eddy viscosity in the wake regions too much and results in an overpredicted drag force. Hence, SST-URANS is not suitable for predicting vortical structures and coherent motion in turbulent flow for blunt body. The SST-DDES was selected for the remaining decay and VIM simulations.

Free-Decay Tests

The free-decay tests contain sway test and yaw test. In sway test, platform was prescribed to an initial linear velocity in Y axis and oscillated freely in the absence of inflow. Similarly, an initial rotation velocity in Z rotation was given to the platform in yaw test. Fig. 6 shows the time history and Fast Fourier Transport (FFT) for decay test. As shown in Fig. 6 (b) and (d), the peak frequencies of CFD in blue solid line agree well with experiment in red dash line both in sway and yaw test, which indicates the effective linear and rotation stiffness between simulation and experiment is identical.

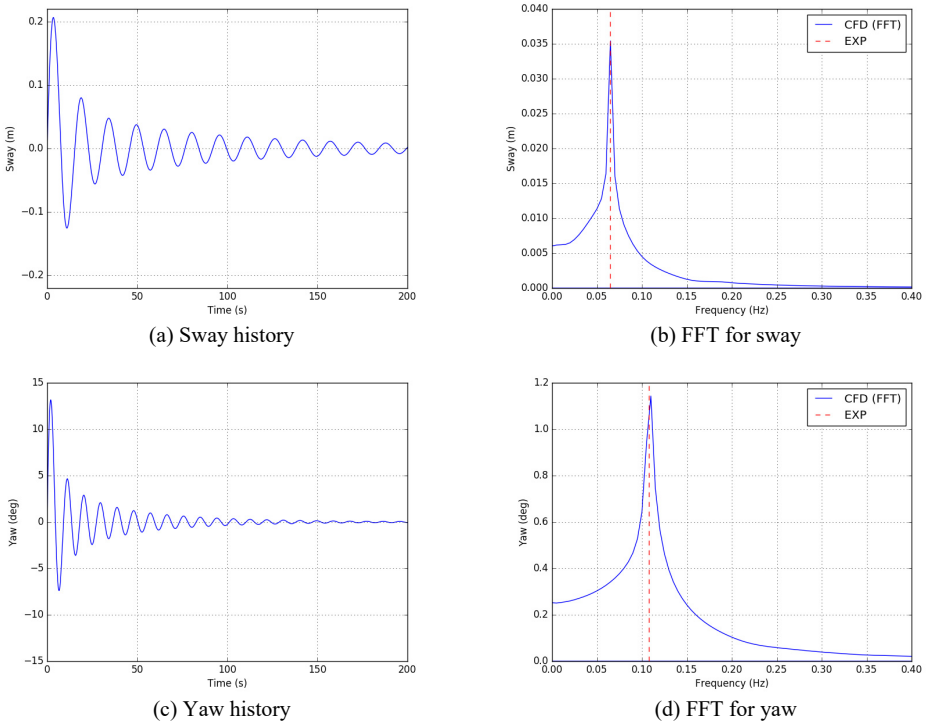

(a) Sway history (b) FFT for sway

(c) Yaw history (d) FFT for yaw

Fig. 6. Free-decay test for sway and yaw

VIM Tests

Five different reduced velocities U_r =5/6/7/8/9 were investigated in the VIM tests. The reduced velocities were computed based on the characteristic diameter of the outer cylinder D=0.36m. Only 0° current heading was investigated for now. Note that the definition of current heading differs from the traditional study of flow past fixed square cylinder. The 0° condition in VIM actually corresponded to the 45° condition of square cylinder.

A typical simulation time of 300s was applied for all cases except U_r=5 and 6. In these two cases, a transient behavior is observed, as shown in Fig. 7. The sway response is small at the beginning of simulation. After the transient stage, the sway motion become modulated strong. The transient stage at lower reduced velocity is much longer (200s for U_r=5 and 150s for U_r=6) than others. Therefore, an extra 100s time was extended for cases U_r=5 and 6.

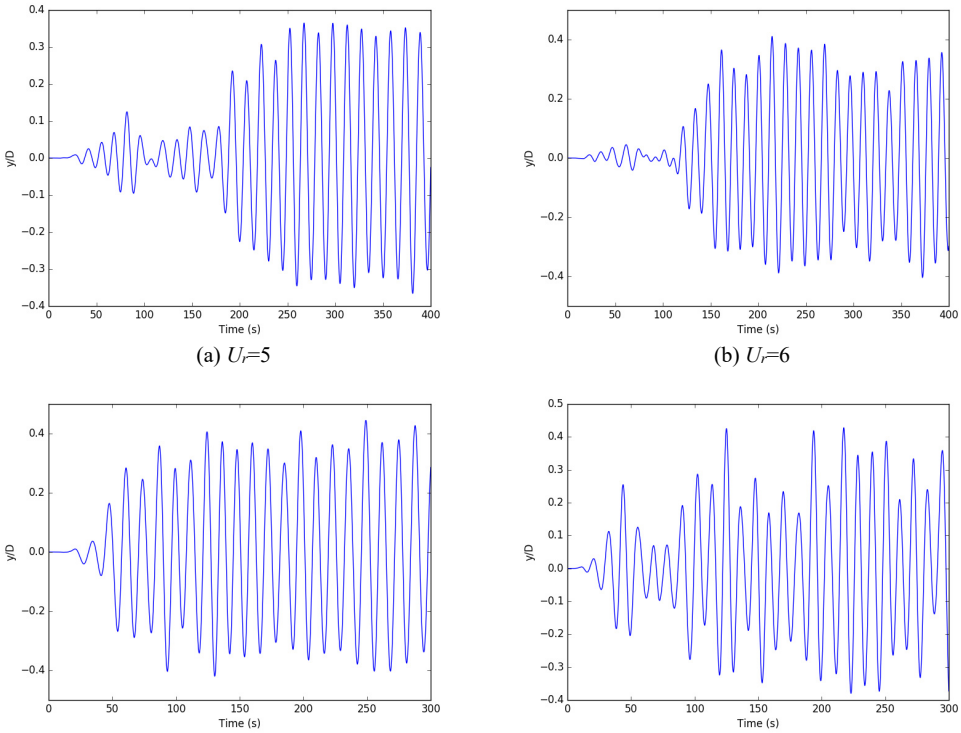

(a) U_r=5 (b) U_r=6

(c) U_r=7 (d) U_r=9

Fig. 7. Time histories of sway for different reduced velocities

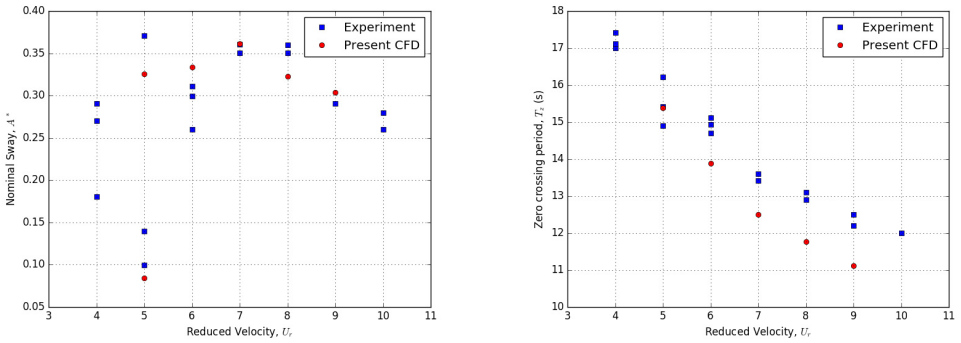

(a) nominal sway (b) zero crossing period

Fig. 8. Comparison of experiment and CFD results

Fig. 8 shows the nominal sway and zero crossing period at different reduced velocities. The statistics range truncates the transient stage and covers at least 18 oscillation cycles (14 for U_r=5). The nominal sway A^* is defined as $A^*=\sqrt{2}\mathrm{RMS}(y/D)$. For the U_r=5 case, statistical calculations of sway response were performed in two ranges: the early transient stage and the post-transient stage. A^* for two stages are 0.083 and 0.325, respectively, which implies two distinguished VIM response regimes exist at U_r=5. Model test also shows two different A^* in repeat towing tests for U_r=5.

Fig. 9 shows the FFT of sway and yaw motions at different reduced velocities. Transient stage for all cases were truncated. Peaks for sway and yaw occur at the same frequency for all cases, suggesting that yaw motions are induced by vortex shedding. Particularly, the peak frequency at U_r=5 is equal to the natural sway frequency. As reduced velocity increases, frequency peak becomes larger and moves away from the natural sway frequency. Interestingly, there is an extra weaker peak frequency for yaw at U_r=8 and 9. This frequency is also observed in sway motion, with much weaker energy. The cause of the extra frequency is still unclear to the author and need to be further investigated.

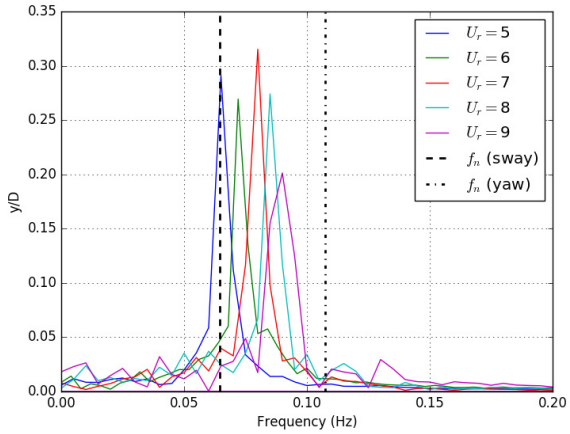

(a) Sway

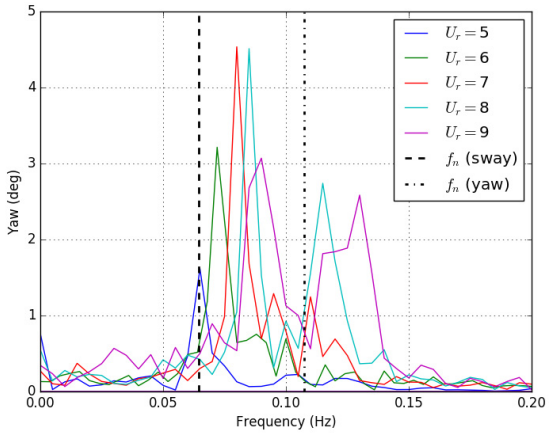

(b) Yaw

Fig. 9. FFT of sway and yaw for VIM tests

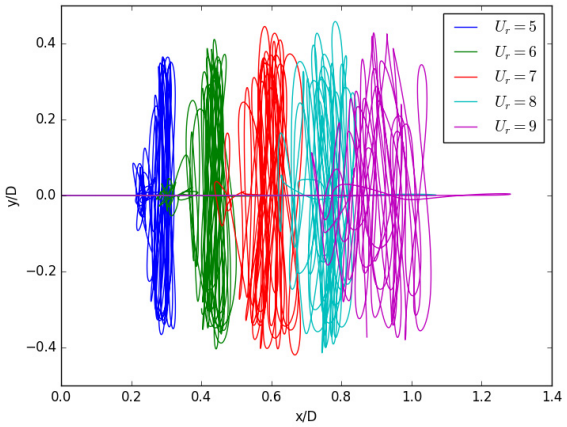

Fig. 10. Motion trajectories of center of mass at different reduced velocities

Fig. 10 shows the plane view of motion trajectories of the model. The drag of model is increasing when reduced velocity increases, resulting in larger offset in X direction. The non-dimensioned sway y/D reaches a maximum value of about 0.4 for all cases. For case U_r=9, a larger surge (in-line) oscillation amplitude is observed. This is caused by the extra yaw frequency that changes the vortex shedding patterns, hence wake structures and pressure in the wake regions.

CONCLUSIONS

A new conceptual design called PC Semi brought by HOE was selected as the basis model to numerically study the mechanism behind VIM for deep draft multi-column platforms. The PC Semi consists of four pair columns that distinguished from conventional DDS. All simulations were performed by the CFD solver naoe-FOAM-SJTU. Turbulence was modeled by the hybrid RANS-LES method SST-DDES. Platform motion was handled by a 6DOF motion solver together with dynamic overset grid technique. Mooring system was solved by considering the coupling effects between linear and rotation stiffness.

Two turbulence models, SST-DDES and SST-URANS, were used in drag test. Results show that SST-DDES is capable in predicting both drag and wake structures more accurate than SST-URANS. Decay tests for both sway and yaw were performed and natural periods of free oscillation were verified with model test, indicating that the current mooring system configuration in numerical simulation can provide same effective stiffness with that in model test and is ready for VIM tests. VIM tests at different reduced velocities were performed after the effective stiffness of the mooring configuration was verified. Two distinguished VIM response regimes were observed in both experiment and simulation at U_r=5. Yaw motions were induced by the vortex shedding and oscillate at the same frequency with sway motions. For high reduced velocity (U_r=8 and 9), two frequency of yaw oscillations were found.

This preliminary study of DDS VIM only investigated the effects of reduced velocities. Current heading is also an important aspect to VIM characteristics due to different Strouhal numbers for different incident angle of square cylinder. Scaling effect is another research hotspot for VIM. These should be consider as parts of the future study.

ACKNOWLEDGEMENTS

This work is supported by the National Natural Science Foundation of China (51379125, 51490675, 11432009, 51579145), Chang Jiang Scholars Program (T2014099), Shanghai Excellent Academic Leaders Program (17XD1402300), Shanghai Key Laboratory of Marine Engineering (K2015-11), Program for Professor of Special Appointment (Eastern Scholar) at Shanghai Institutions of Higher Learning (2013022), Innovative Special Project of Numerical Tank of Ministry of Industry and Information Technology of China (2016-23/09) and Lloyd's Register Foundation for doctoral student, to which the authors are most grateful.

REFERENCES

Antony, A, Vinayan, V, Holmes, S, Spernjak, D, Kim, SJ, and Halkyard, J (2015a). "VIM Study for Deep Draft Column Stabilized Floaters," *Offshore Technol Conf*, Houston, Texas, USA. OTC-25837-MS.

Antony, A, Vinayan, V, Halkyard, J, Kim, S-J, Holmes, S, and Spernjak, D (2015b). "A CFD based analysis of the Vortex Induced Motion of deep-draft semisubmersibles," *Proc Twenty-Fifth 2015 Int Ocean Polar Eng Conf*, Kona, Big Island, Hawaii, USA, ISOPE, (3) 1048–1055.

Chen, C-R, and Chen, H-C (2016). "Simulation of vortex-induced motions of a deep draft semi-submersible in current," *Ocean Eng*, 118, 107–116.

Dijk, RRT van, Magee, A, Perryman, S, and Gebara, J (2003a). "Model test experience on vortex induced vibrations of Truss Spars," *Offshore Technol Conf*, Houston, Texas, USA, OTC-15242-MS.

Dijk, RRT van, Fourchy, P, Voogt, A, and Mirza, S (2003b). "The effect of mooring system and sheared currents on vortex induced motions of truss Spars," *Proc 22nd Int Conf Offshore Mech Arct Eng*, Cancun, Mexico, OMAE2003-37151.

Gonçalves, RT, Nishimoto, K, Rosetti, GF, Fujarra, ALC, and Oliveira, AC (2011). "Experimental study on vortex-induced motions (VIM) of a large-volume semi-submersible platform," *Proc ASME 2011 30th Int Conf Ocean Offshore Arct Eng*, Rotterdam, The Netherlands, OMAE2011-49010.

Kara, M, Kaufmann, J, Gordon, R, Sharma, P, and Lu, J (2016). "Application of CFD for Computing VIM of Floating Structures," *Offshore Technol Conf*, Houston, Texas, USA, OTC-26950-MS.

Kim, J-W, Magee, A, and Guan, KYH (2011). "CFD simulation of flow-induced motions of a multi-column floating platform," *Proc ASME 2011 30th Int Conf Ocean Offshore Arct Eng*, Rotterdam, The Netherlands, OMAE2011-49437.

Kim, SJ, Spernjak, D, Holmes, S, Vinayan, V, and Antony, A (2015). "Vortex-Induced Motion of Floating Structures: CFD Sensitivity Considerations of Turbulence Model and Mesh Refinement," *Proc ASME 2015 34th Int Conf Ocean Offshore Arct Eng*, St. John's, Newfoundland, Canada, OMAE2015-42221.

Magee, A, Sheikh, R, Guan, KYH, Choo, JTH, Malik, AMA, Ghani, MPA, and Abyn, H (2011). "Model tests for VIM of multi-column floating platforms," *Proc ASME 2011 30th Int Conf Ocean Offshore Arct Eng*, Rotterdam, The Netherlands, OMAE2011-49151.

Menter, FR, Kuntz, M, and Langtry, R (2003). "Ten years of industrial experience with the SST turbulence model," *Turbul Heat Mass Transf*, 4(1), 625–632.

Noack, RW, Boger, DA, Kunz, RF, and Carrica, PM (2009). "Suggar++: An improved general overset grid assembly capability," *19th AIAA Comput Fluid Dyn Conf*, San Antonio, Texas, USA, AIAA 2009-3992.

Norberg, C (1993). "Flow around rectangular cylinders: Pressure forces and wake frequencies," *J Wind Eng Ind Aerodyn*, 49(1–3), 187–196.

Norberg, C (1994). "An experimental investigation of the flow around a circular cylinder: influence of aspect ratio," *J Fluid Mech*, 258, 287–316.

Norberg, C, and Sunden, B (1987). "Turbulence and Reynolds number effects on the flow and fluid forces on a single cylinder in cross flow," *J Fluids Struct*, 1(3), 337–357.

Shen, Z, and Wan, DC (2013). "RANS computations of added resistance and motions of a ship in head waves," *Int J Offshore Polar Eng*, ISOPE, 23(4), 263–271.

Shen, Z and Wan, DC (2012). "The manual of CFD solver for ship and ocean engineering flows: naoe-FOAM-SJTU," Shanghai, China, Shanghai Jiao Tong University.

Shen, Z, Wan, DC, and Carrica, PM (2015). "Dynamic overset grids in OpenFOAM with application to KCS self-propulsion and maneuvering," *Ocean Eng*, 108, 287–306.

Vinayan, V, Antony, A, Halkyard, J, Kim, S-J, Holmes, S, and Spernjak, D (2015). "Vortex-induced motion of deep-draft semisubmersibles: A CFD-based parametric study," *Proc ASME 2015 34th Int Conf Ocean Offshore Arct Eng*, St. John's, Newfoundland, Canada, OMAE2015-42209.

Waals, OJ, Phadke, AC, and Bultema, S (2007). "Flow induced motions of multi column floaters," *Proc 26th Int Conf Offshore Mech Arct Eng*, San Diego, California, USA, 1, 669–678.

Zhao, W, and Wan, DC (2016a). "Detached-Eddy Simulation of Flow Past Tandem Cylinders," *Appl Math Mech*, 37(12), 1272–1281.

Zhao, W, and Wan, DC (2016b). "Numerical computations of Spar vortex-induced motions at different current headings," *Proc Twenty-Sixth Int Ocean Polar Eng Conf*, Rhodes, Greece, ISOPE, 3, 1122–1127.

Zhao, W, and Wan, DC (2016c). "Numerical study of 3D flow past a circular cylinder at subcritical Reynolds number using SST-DES and SST-URANS," *Chin J Hydrodyn*, 31(1), 1–8.

Zou, J, Poll, P, Roddier, D, Tom, N, and Peiffer, A (2013). "VIM testing of a paired column semi submersible," *Proc ASME 2013 32nd Int Conf Ocean Offshore Arct Eng*, Nantes, France, OMAE2013-10001.